Electronic Supplementary Material (ESI) for Inorganic Chemistry Frontiers.

Supporting Information

Efficient Oxygen Evolution Reaction by Ru(II) Polypyridyl Complex based AIEgen

Snehadrinarayan Khatua[a] Monosh Rabha[a], Sreenivasan Nagappan[bc], Bhaskar Sen[a], Khanindram Baruah[a], and Subrata Kundu[bc]**

[a]*Centre for Advanced Studies, Department of Chemistry, North-Eastern Hill University, Shillong, Meghalaya 793022, India*

[b]*Academy of Scientific and Innovative Research (AcSIR), Ghaziabad-201002, India.*

[c]*Electrochemical Process Engineering (EPE) Division, CSIR-Central Electrochemical Research Institute (CECRI), Karaikudi - 630 003, INDIA*

**Corresponding Author: snehadri@gmail.com; skhatua@nehu.ac.in*

skundu@cecri.res.in; kundu.subrata@gmail.com

This file contains 18 pages in which the details of reagents, methods of synthesis, electrochemical characterizations, electrochemical results, and characterizations like NMR UV and Solvatochromism spectrum of prepared samples.

No. of Figures: 25

No. Tables: 4

Table of Contents		
Sl. No.	**Content**	**Page No.**
1.	List of compounds used in this study	S3
2.	Synthesis of complexes **Ru-1** to **Ru-6**	S3-S4
3.	^{1}HNMR spectra of **Ru-1** to **Ru-6**	S5-S7
4.	NMR spectra of **DAP**	S7-S8
5.	ESI-MS of **DAP**	S8
6.	NMR spectra of **L4**	S9
7.	ESI-MS of **L4**	S10
8.	NMR spectra of **Ru4**	S10-S11
9.	ESI-MS of **Ru4**	S11
10.	Crystal Parameters	S12-S13
11.	UV spectra of **Ru-4** in CH_3CN–water and CH_3CN–PEG mixture	S14
12.	Solvent Dependent luminescence study	S14
13.	Raman spectra of **Ru-4**	S15
14.	EDX spectra of **Ru-4**	S15
15.	High-resolution XPS spectra of of **Ru-4**	S16
16.	BET surface area curves	S16
17.	Bar diagram for the overpotential values	S17
18.	OER study of the state-of-art catalyst and carbon cloth	S17
19.	Plausible mechanism	S18
20.	GC-MS setup	S18

Chart S1. List of Compounds used in this study

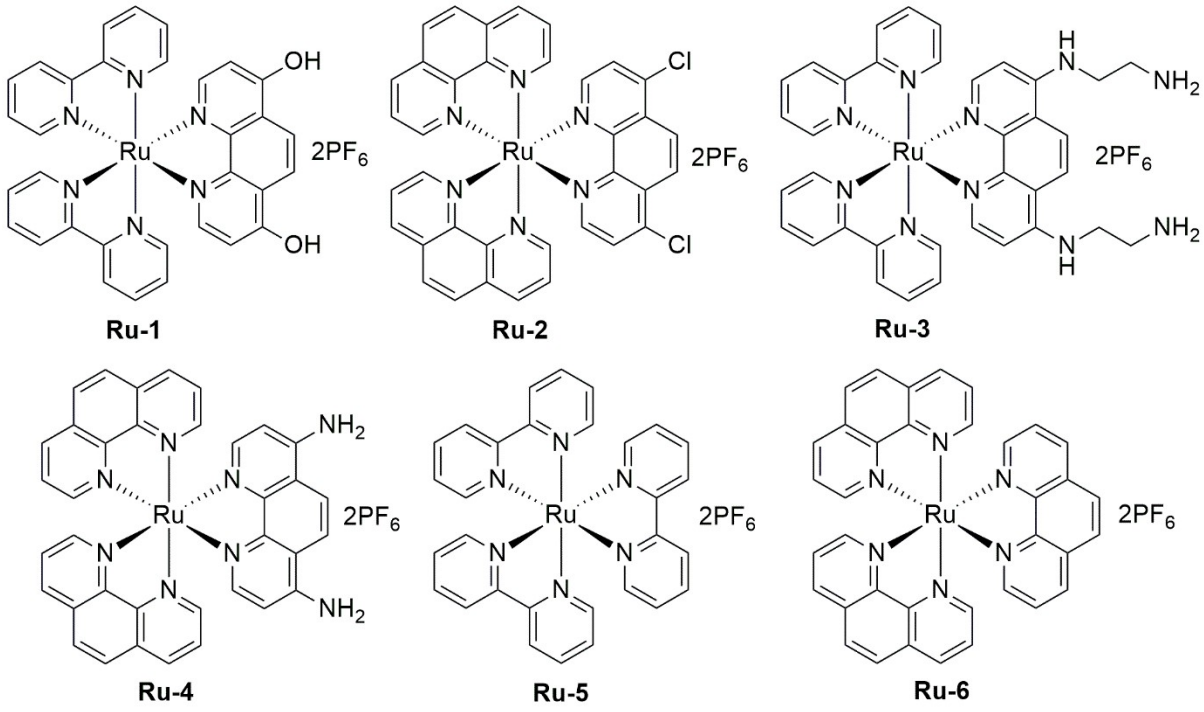

Synthesis of complexes Ru-1 to Ru-6

The desired ligands and complexes **Ru-1**, **Ru-2, Ru-3, Ru-5 and Ru-6** were prepared according to reported literature procedures and characterized by ^{1}H NMR spectroscopy.[1-4] Complex **Ru-4** was characterized by Single Crytal X-Ray Diffraction, NMR, ESI-MS and FT-IR.

Complex **Ru-1**: The complex was synthesized following the reported procedure.[1] Yield: 58 mg (57%). Melting point (MP): > 300 °C. ^{1}H NMR (400 MHz, Acetone-d_6) δ (ppm) 8.48 (m, 4H), 8.29 (s, 1H), 8.04 (td, J = 6.4, 1.6 Hz, 2H), 7.97 (td, J = 6.4, 1.6 Hz, 2H), 7.84 (d, J = 5.6 Hz, 1H), 7.68 (d, J = 6.4 Hz, 1H), 7.64 (d, J = 6.4 Hz, 1H), 7.39 (m, 2H), 7.23 (m, 2H), 7.08 (d, J = 6 Hz, 1H).

Complex **Ru-2**: The complex was synthesized following the reported procedure.[2] Yield: 36 mg (58%). Melting point (MP): > 300 °C. ^{1}H NMR (400 MHz, Acetone-d_6) δ (ppm) 8.80 (t, J = 7.6 Hz, 2H), 8.70 (s, 1H), 8.52 (d, J = 5.2 Hz, 1H), 8.46 (d, J = 6.4 Hz, 1H), 8.42 (s, 2H), 8.37 (d, J = 5.2 Hz, 1H), 7.96 (d, J = 5.6 Hz, 1H), 7.82-7.78 (m, 2H).

Complex **Ru-3**: The complex was synthesized following the reported procedure.[3] Yield = 0.23 g (60 %). Melting point = >300°C. ^{1}H NMR (400 MHz, DMSO-d_6): δ (ppm) = 8.84–8.80 (m, 2H, $H_{3',3''}$), 8.31 (s, 1H, H_5), 8.15 (t, J = 8.5 Hz, 1H), 8.07 (t, J = 7.2 Hz, 3H,), 7.85 (d, J = 5.2 Hz, 1H), 7.72 (d, J = 5.1 Hz, 3H), 7.52 (t, J = 7.1 Hz, 1H), 7.41 (t, J = 7.1 Hz, 1H), 7.29 (d, J = 6.4 Hz, 1H), 6.81 (d, J = 6.6 Hz, 1H), 3.55-3.54 (m, 2H), 3.10 (t, J = 6.2 Hz, 2H).

Complex **Ru-5**: The complex was synthesized following the reported procedure.[4] Yield: 63 mg (82%). Melting point (MP): > 300 °C. ^{1}H NMR (400 MHz, DMSO-d_6) δ (ppm) 8.85 (d, J = 8.4 Hz, 1H), 8.18 (t, J = 7.6 Hz, 1H), 7.73 (d, J = 5.6 Hz, 1H), 7.53 (t, J = 6.4 Hz, 1H).

Complex **Ru-6**: The complex was synthesized following the reported procedure.[4] Yield: 81 mg (87%). Melting point (MP): > 300 °C. ^{1}H NMR (400 MHz, Acetonitrile-d_3) δ (ppm) 8.63 (d, J = 8.4 Hz, 1H), 8.27 (s, 1H), 8.05 (d, J = 4.8 Hz, 1H), 7.66 (t, J = 8.3, 5.6 Hz, 1H).

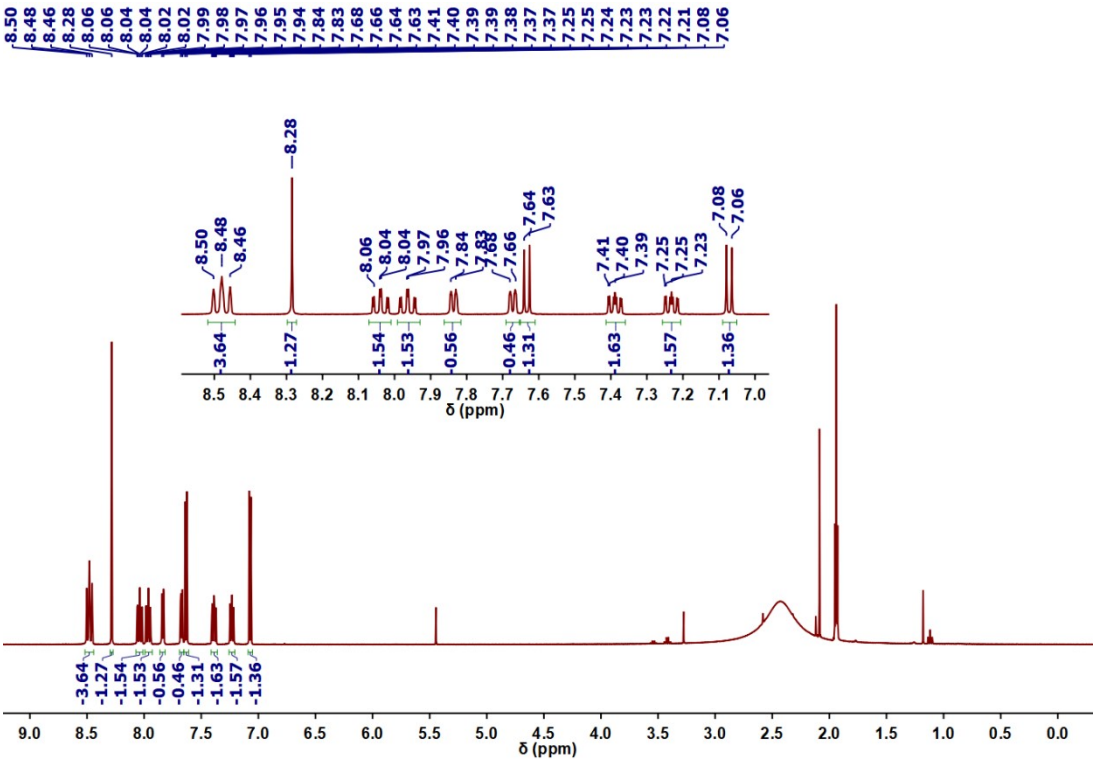

Figure S1: ^{1}H NMR spectrum **Ru-1** in Acetone-d_6 (400 MHz).

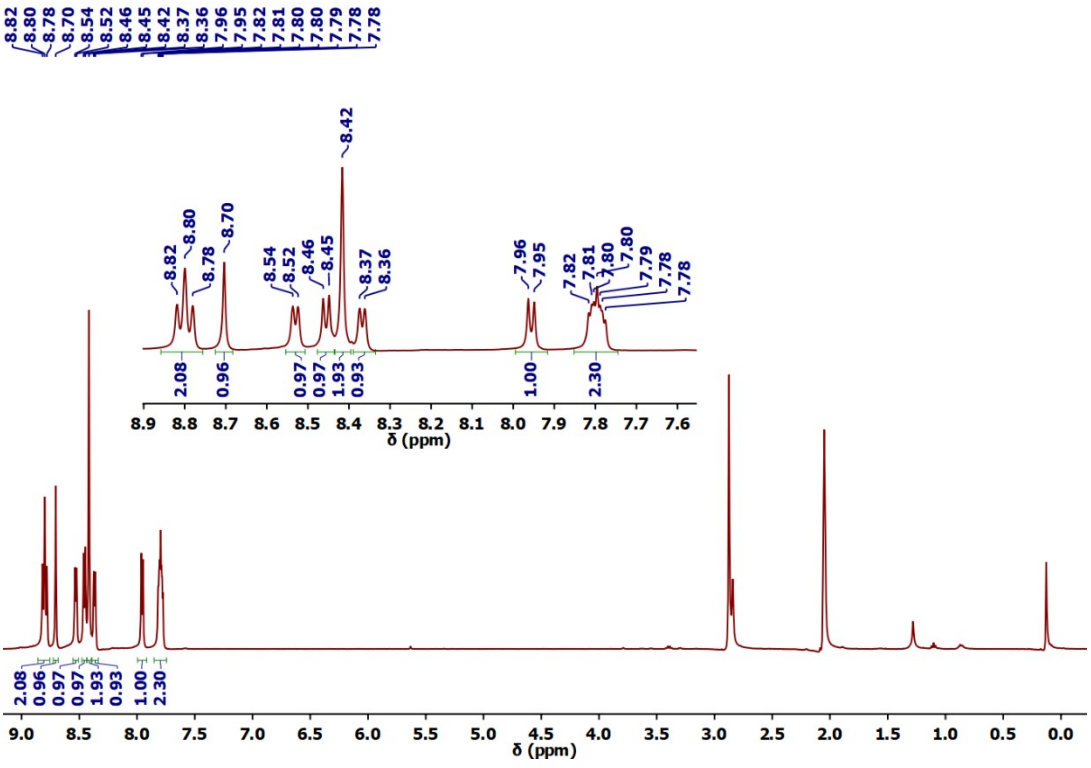

Figure S2: ^{1}H NMR spectrum **Ru-2** in Acetone-d_6 (400 MHz).

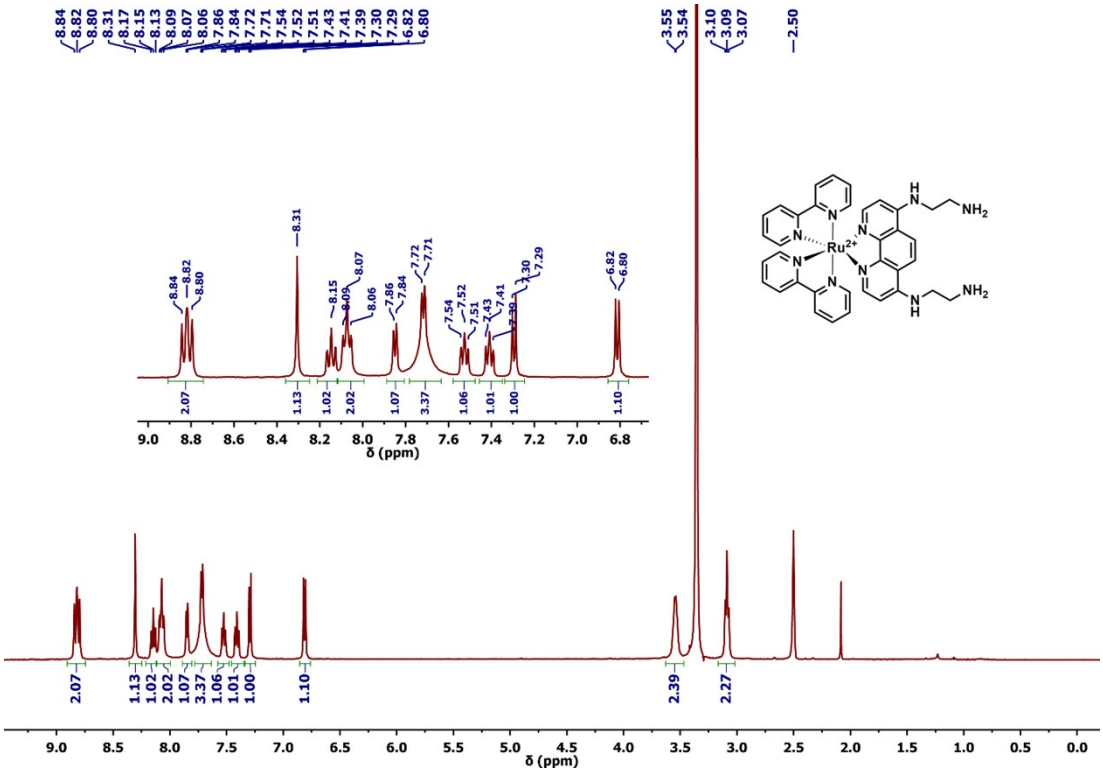

Figure S3: ^{1}H NMR spectrum **Ru-3** in DMSO-d_6 (400 MHz).

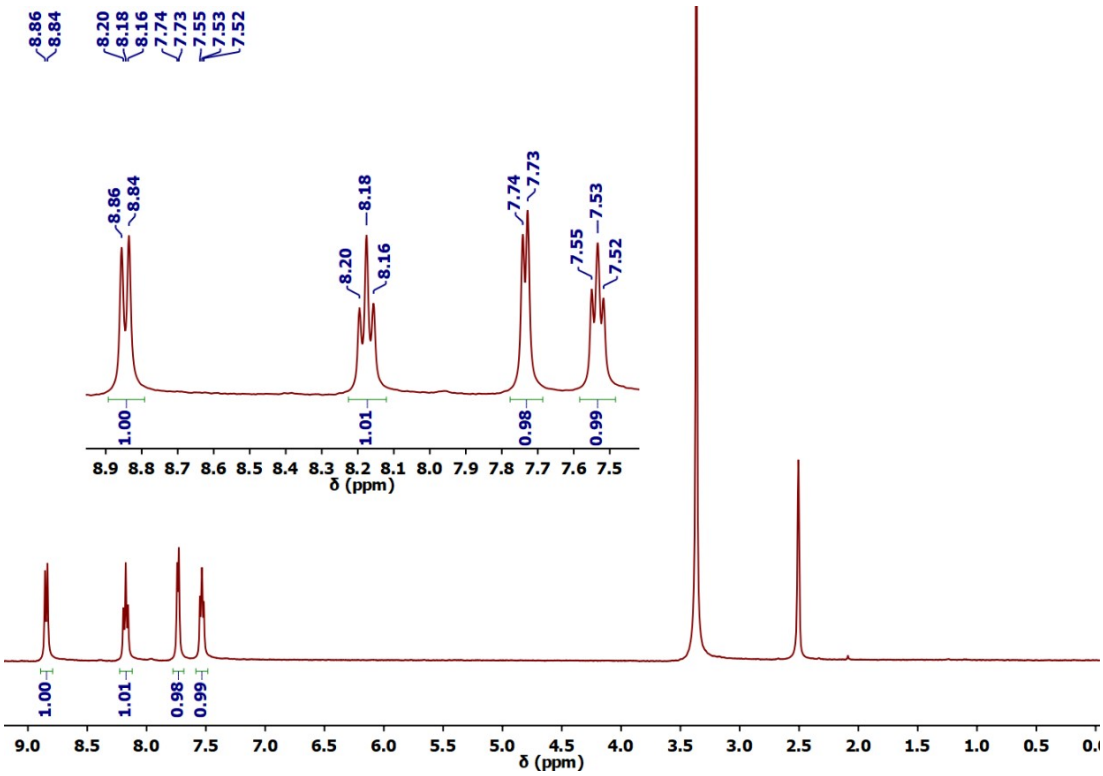

Figure S4: ^{1}H NMR spectrum **Ru-5** in DMSO-d_6 (400 MHz).

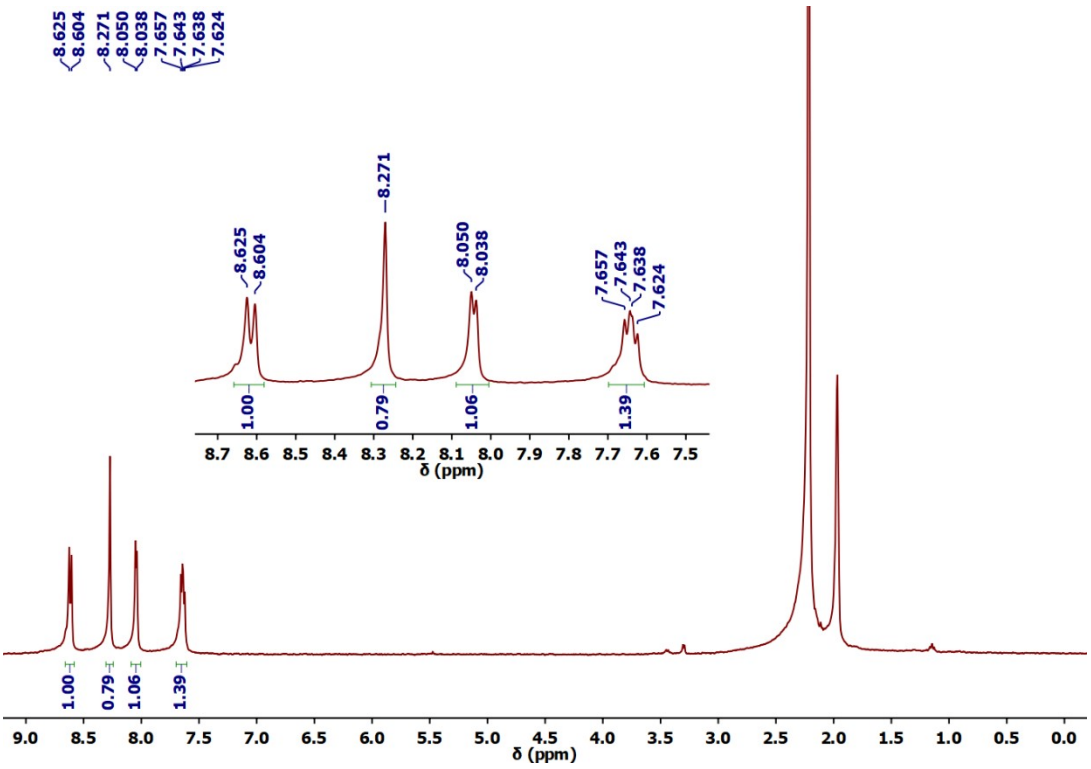

Figure S5: ^{1}H NMR spectrum **Ru-6** in Acetonitrile-d_3 (400 MHz).

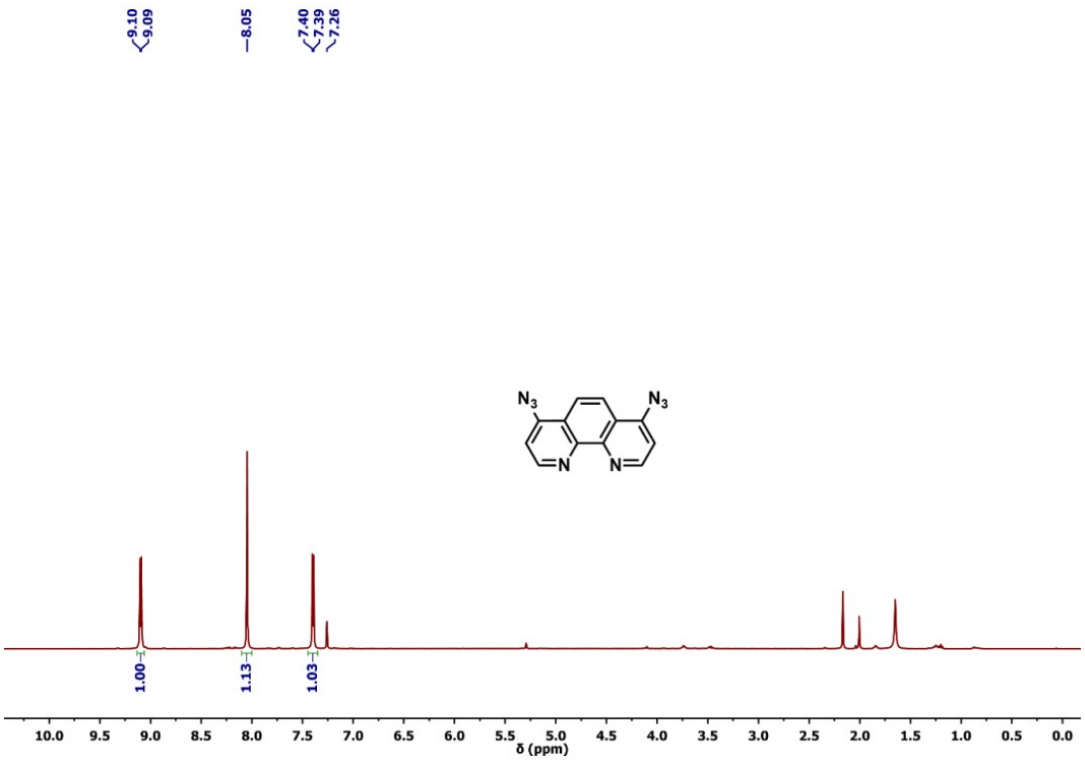

Figure S6: ^{1}H NMR spectrum of **DAP** in $CDCl_3$ (400 MHz).

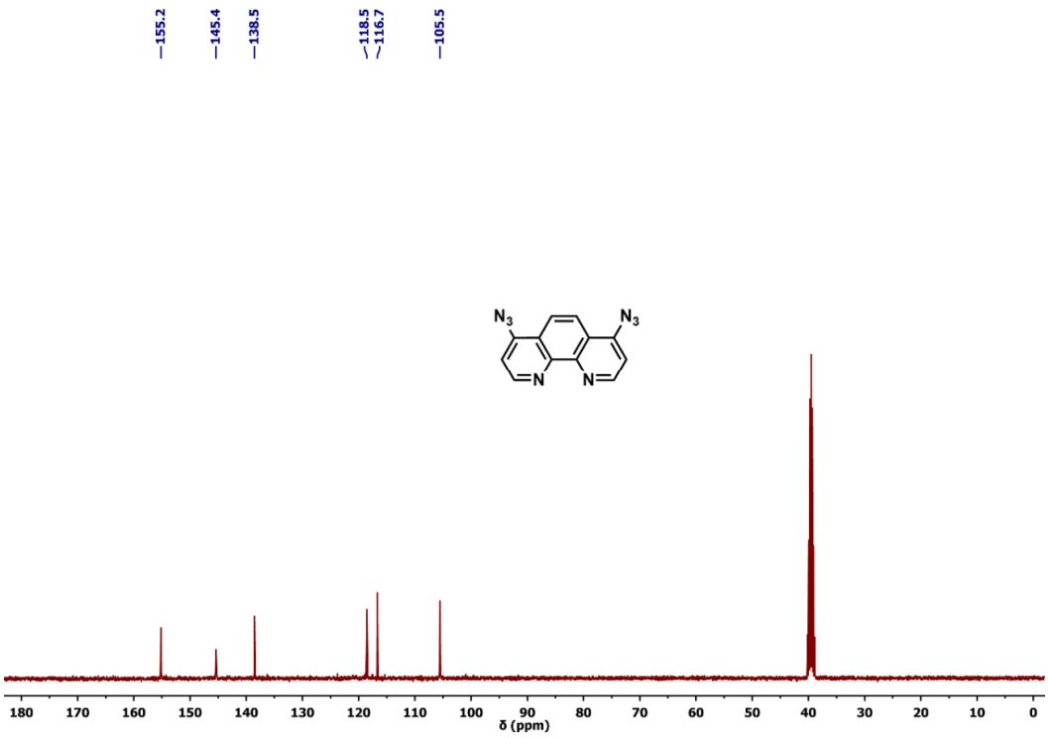

Figure S7: ^{13}C NMR spectrum of **DAP** in $CDCl_3$ (100 MHz).

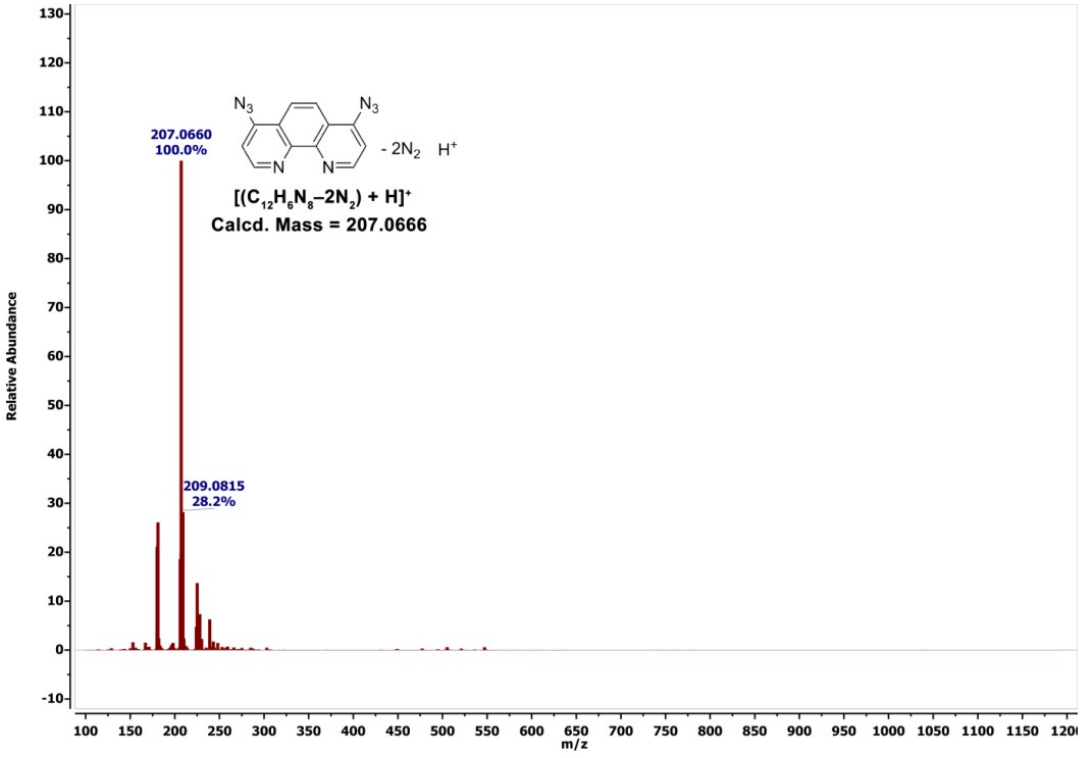

Figure S8: ESI-HRMS spectrum of **DAP** in CH_3OH

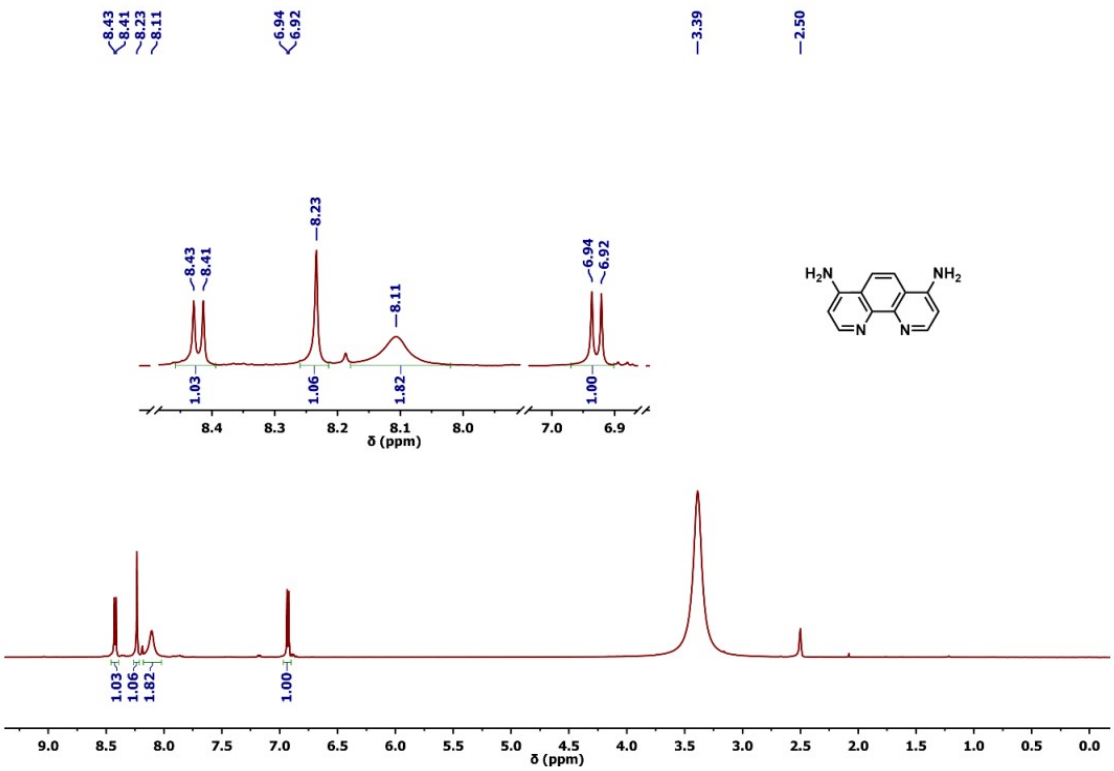

Figure S9: [1]H NMR spectrum of **L4** in DMSO- *d6* (400 MHz).

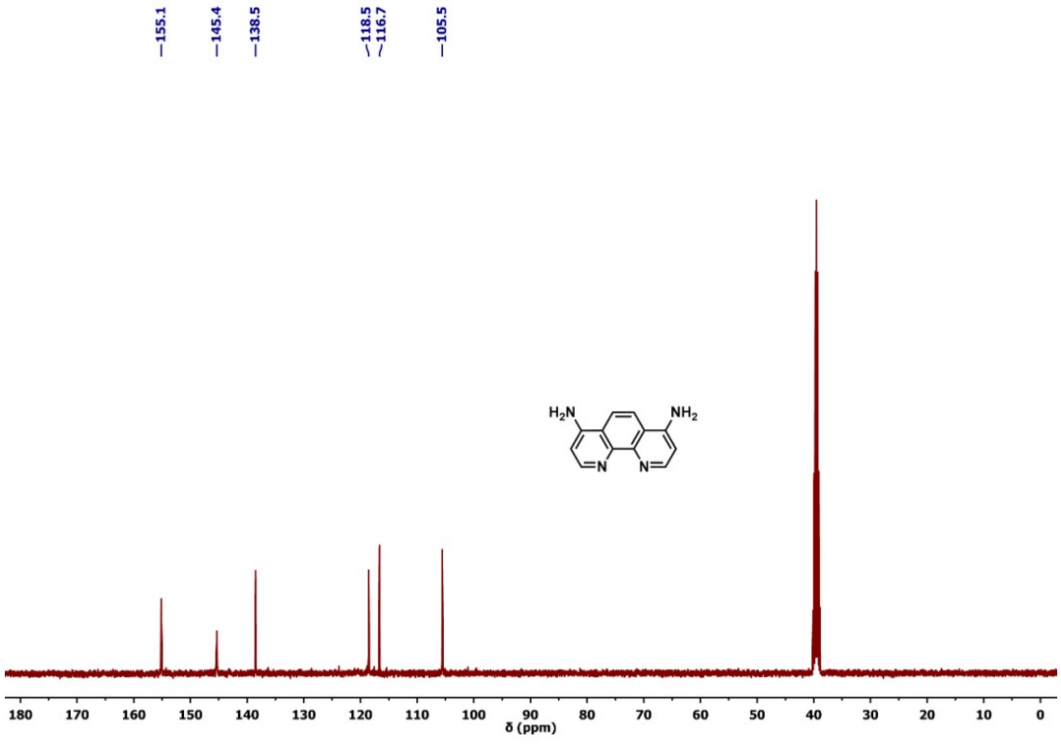

Figure S10: [13]C NMR spectrum of **L4** in DMSO-*d6*(100 MHz).

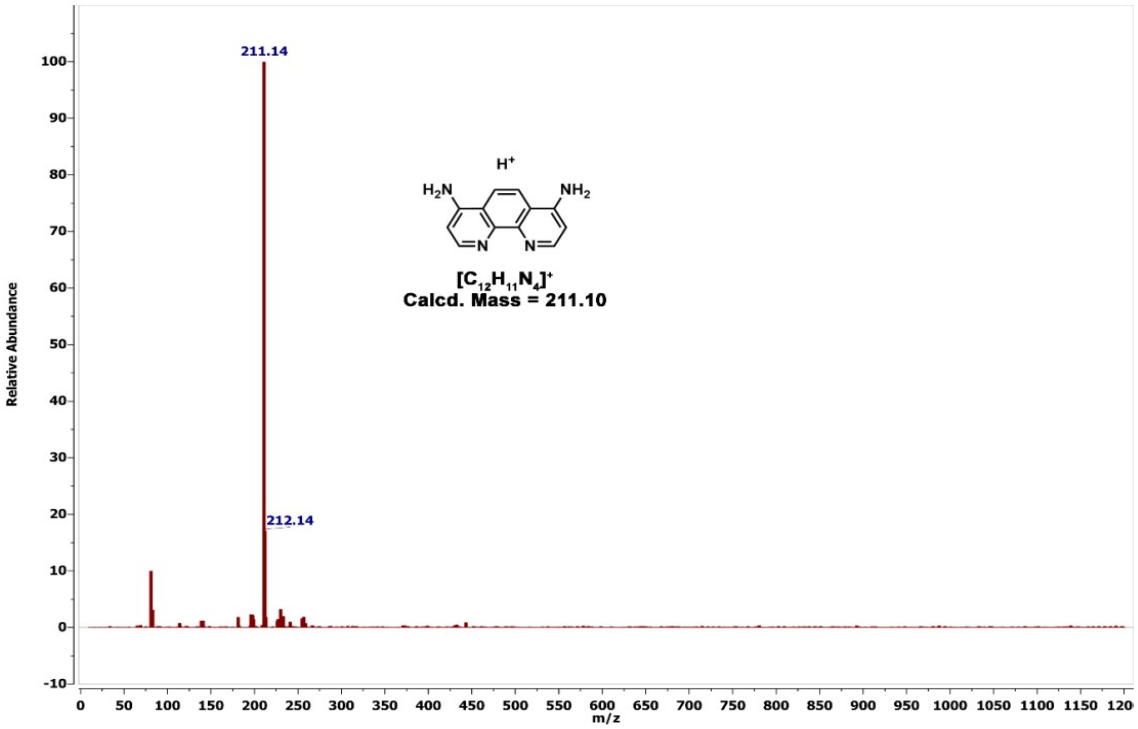

Figure S11: ESI-MS of **L4** in CH_3OH.

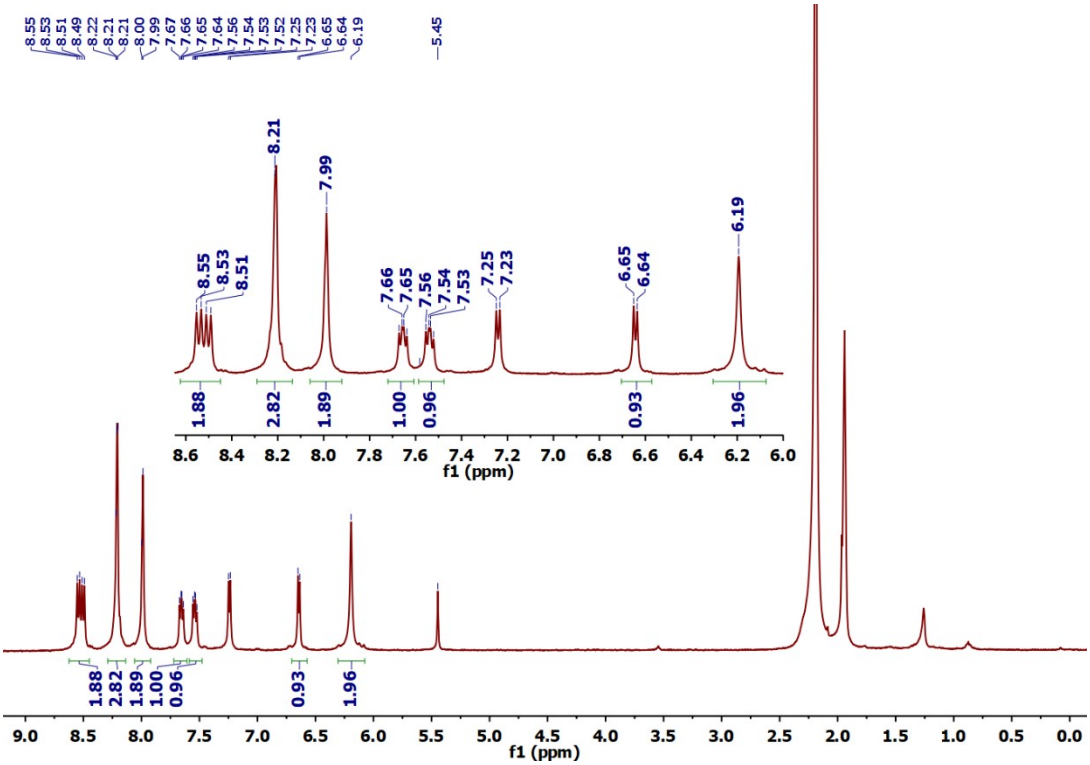

Figure S12: ^1H NMR of **Ru-4** in CD_3CN (400 MHz).

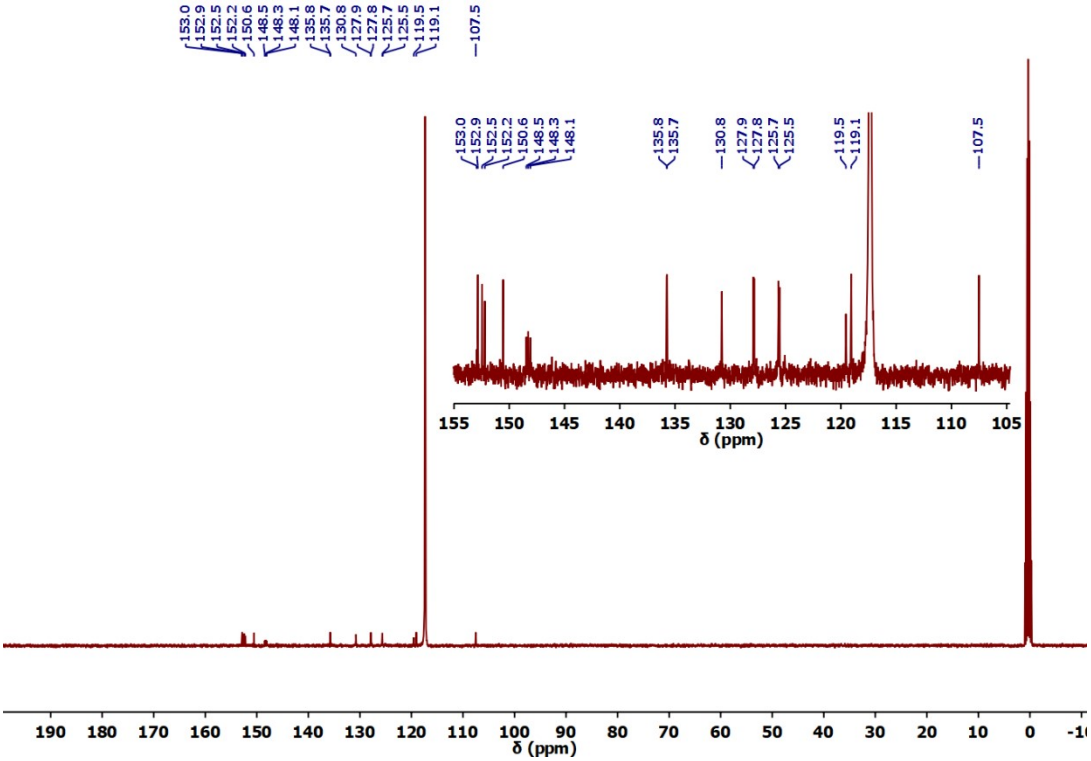

Figure S13: ^{13}C NMR of **Ru-4** in Acetonitrile-d_3 (100 MHz).

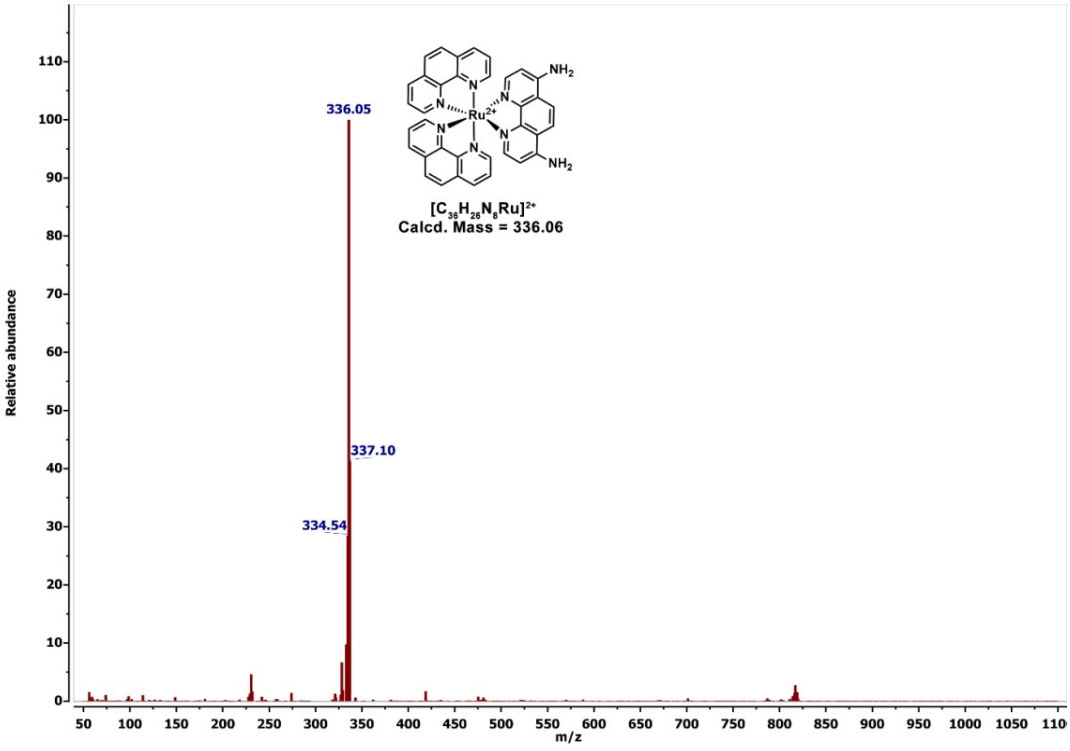

Figure S14: ESI-MS spectrum of **Ru-4** in CH_3CN.

Table S1: Single crystal data and refinement details of **DAP**:

Empirical formula	$C_{13}H_7C_{l3}N_8$
Formula weight	381.62
Temperature	293(2) K
Wavelength	0.71073 Å
Crystal system	Triclinic
Space group	*P*-1
Unit cell dimensions	*a* = 9.1563(11) Å α = 84.532(9)°. *b* = 9.6598(11) Å β = 70.930(11)°. *c* = 9.7144(10) Å γ = 89.659(10)°.
Volume	808.08(17) Å^3
Z	2
Density (calculated)	1.568 Mg/m^3
Absorption coefficient	0.580 mm^{-1}
F(000)	384
Crystal size	0.180 x 0.120 x 0.080 mm^3
Theta range for data collection	3.302 to 26.372°.
Index ranges	-10<=h<=11, -9<=k<=12, -12<=l<=11
Reflections collected	5144
Independent reflections	3271 [*R*(int) = 0.0239]
Completeness to theta = 26.000°	99.4 %
Refinement method	Full-matrix least-squares on F^2
Data / restraints / parameters	3271 / 0 / 217
Goodness-of-fit on F^2	1.034
Final *R* indices [*I*>2sigma(*I*)][a]	*R*1 = 0.0722, w*R*2 = 0.1392
R indices (all data)[a]	*R*1 = 0.1195, w*R*2 = 0.1638
Extinction coefficient	n/a
Largest diff. peak and hole	0.368 and -0.427 e.Å^{-3}

[a] $R1 = \Sigma||F_o| - |F_c||/\Sigma|F_o|$; $wR2 = \{\Sigma[w(F_{o2} - F_{c2})_2]/\Sigma w(F_{o2})_2\}^{1/2}$

Table S2: Single crystal data and refinement details of **Ru-4**:

Empirical formula	$C_{37}H_{27}Cl_3F_{12}N_8P_2Ru$
Formula weight	1081.02
Temperature	293(2) K
Wavelength	0.71073 Å
Crystal system	Monoclinic
Space group	$P\ 2_1/c$
Unit cell dimensions	a = 15.560(2) Å $\alpha = 90°$.
	b = 13.6055(10)Å $\beta = 102.396(13)°$.
	c = 21.302(3) Å $\gamma = 90°$.
Volume	4404.7(9)Å^3
Z	4
Density (calculated)	1.630 Mg/m^3
Absorption coefficient	0.700 mm^{-1}
F(000)	2152
Crystal size	0.250 x 0.210 x 0.120 mm^3
Theta range for data collection	3.151 to 25.054°.
Index ranges	-18<=h<=6, -16<=k<=16, -24<=l<=25
Reflections collected	10785
Independent reflections	6143 [R(int) = 0.0446]
Absorption correction	Semi-empirical from equivalents
Max. and min. transmission	1.00000 and 0.81204
Refinement method	Full-matrix least-squares on F^2
Data / restraints / parameters	6143 / 0 / 568
Goodness-of-fit on F^2	1.033
Final R indices [I>2sigma(I)][a]	$R1$ = 0.0999, $wR2$ = 0.2413
R indices (all data)[a]	$R1$ = 0.1470, $wR2$ = 0.2782
Extinction coefficient	n/a
Largest diff. peak and hole	0.801 and -0.841 e.Å^{-3}

[a] $R1 = \Sigma||F_o| - |F_c||/\Sigma|F_o|$; $wR2 = \{\Sigma[w(F_o^2 - F_c^2)^2]/\Sigma w(F_o^2)^2\}^{1/2}$

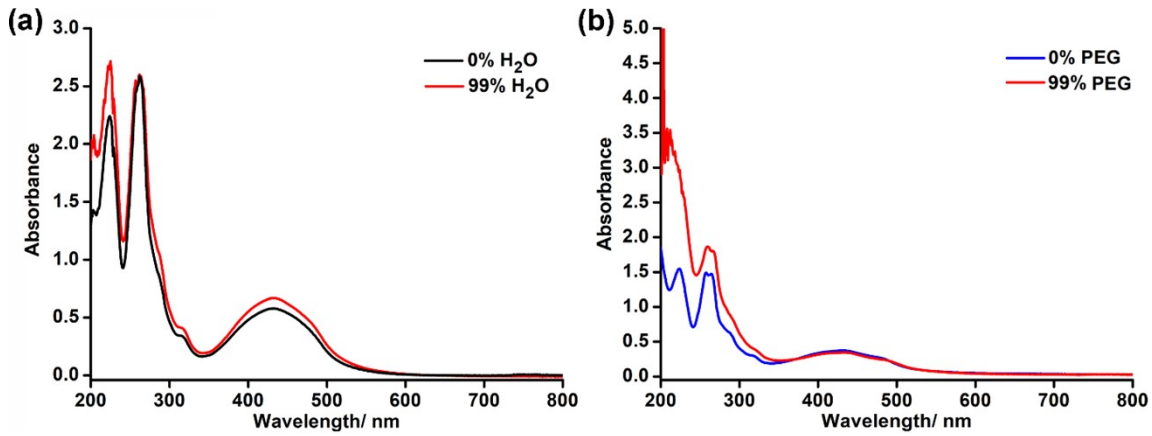

Figure S15: UV-vis spectra of **Ru-4** (25 μM) in 0% and 90% (a) H_2O and (b) PEG.

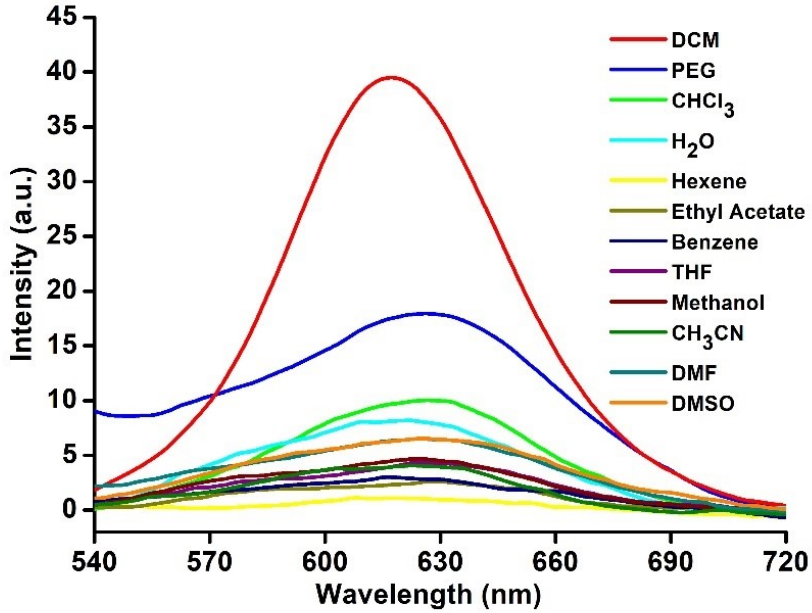

Figure S16: Solvatochromism spectra of **Ru-4** (25 μM) in different solvents.

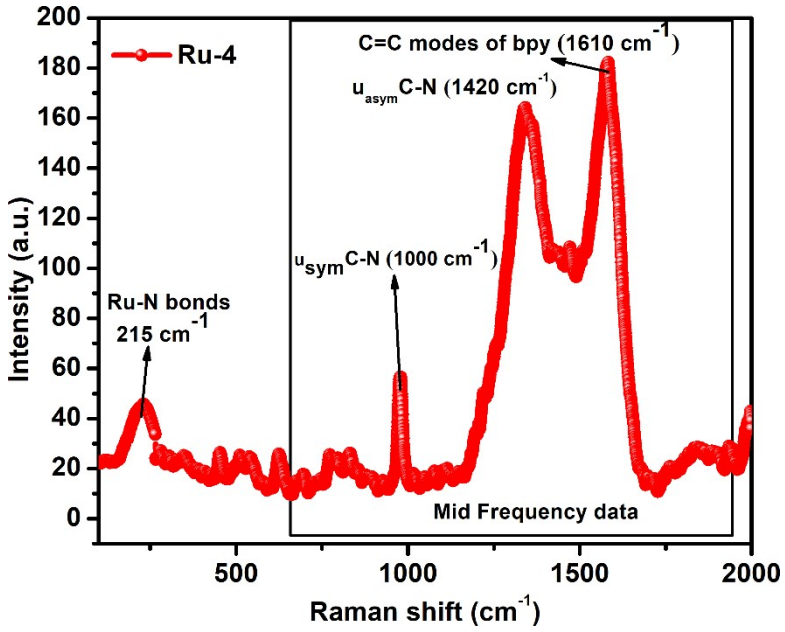

Figure S17: Raman spectra of **Ru-4.**

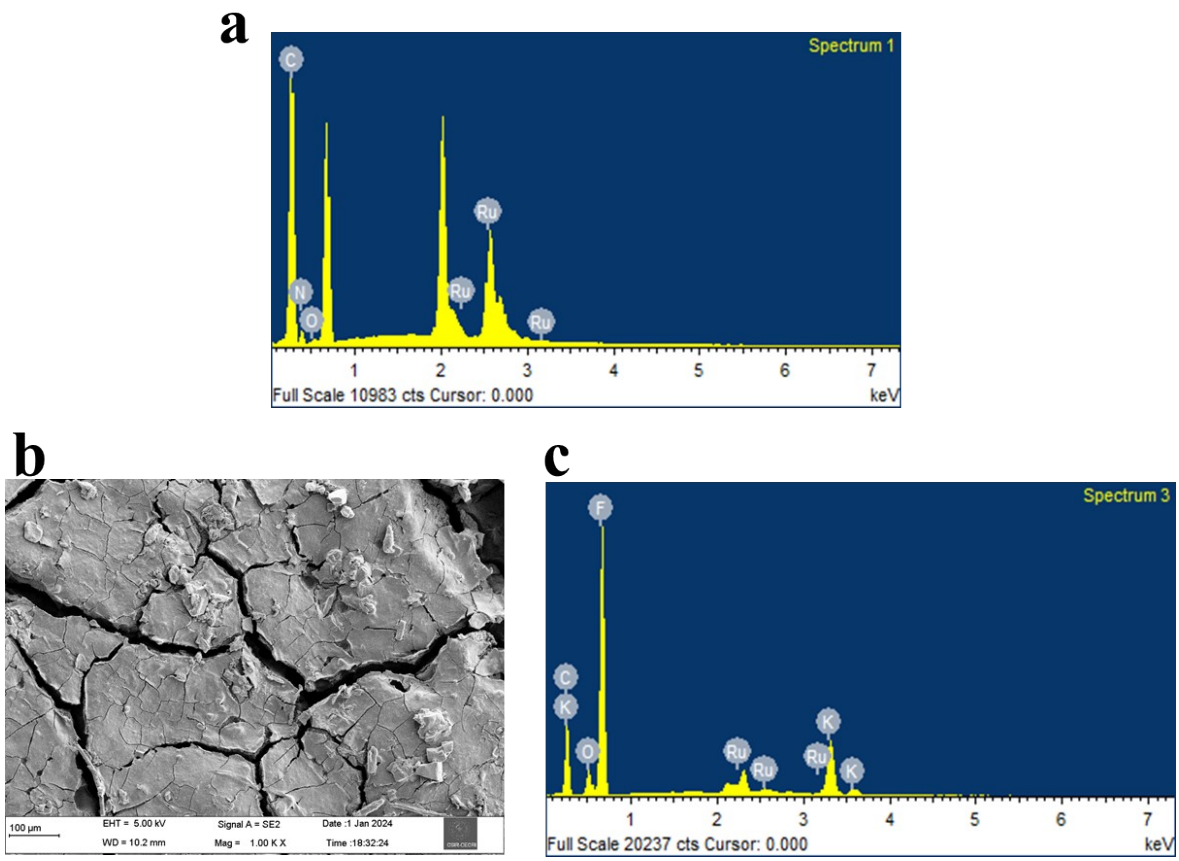

Figure S18: EDX spectra of **Ru-4** (a-b) SEM images of before OER, (c) EDX of before OER, (d-e) SEM images of after OER, and (b) EDX of after OER study.

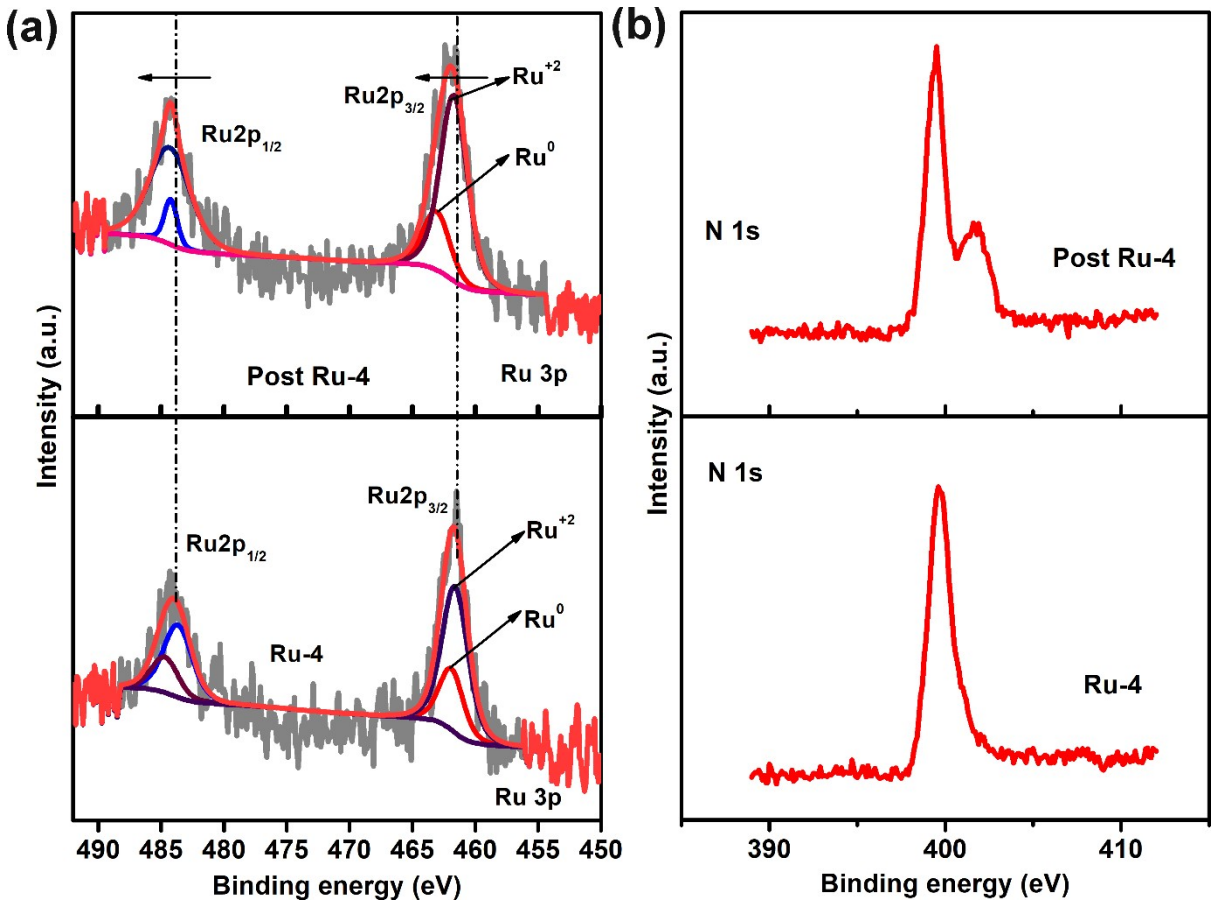

Figure S19: High-resolution XPS spectra of of **Ru-4**.

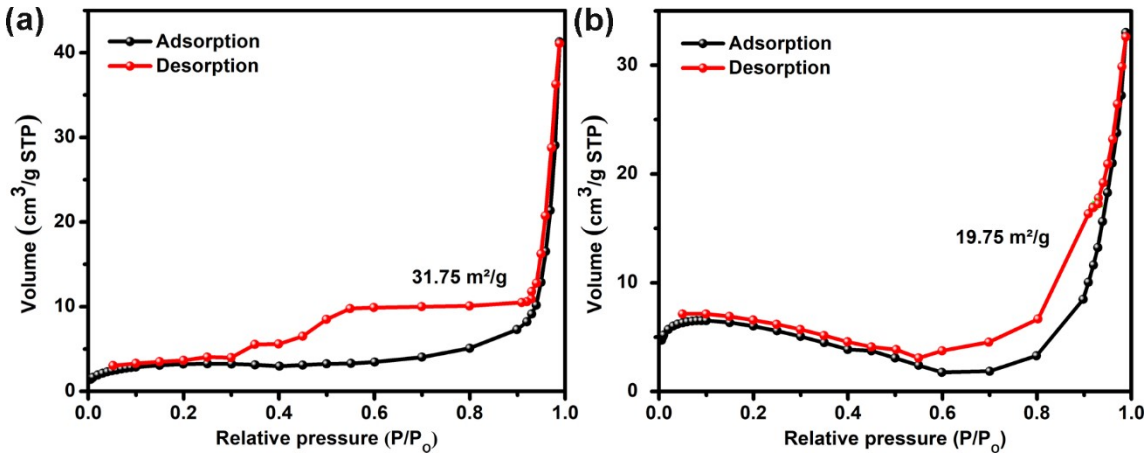

Figure S20: BET surface area curves of (a) **Ru-4** and (b) **Ru-3.**

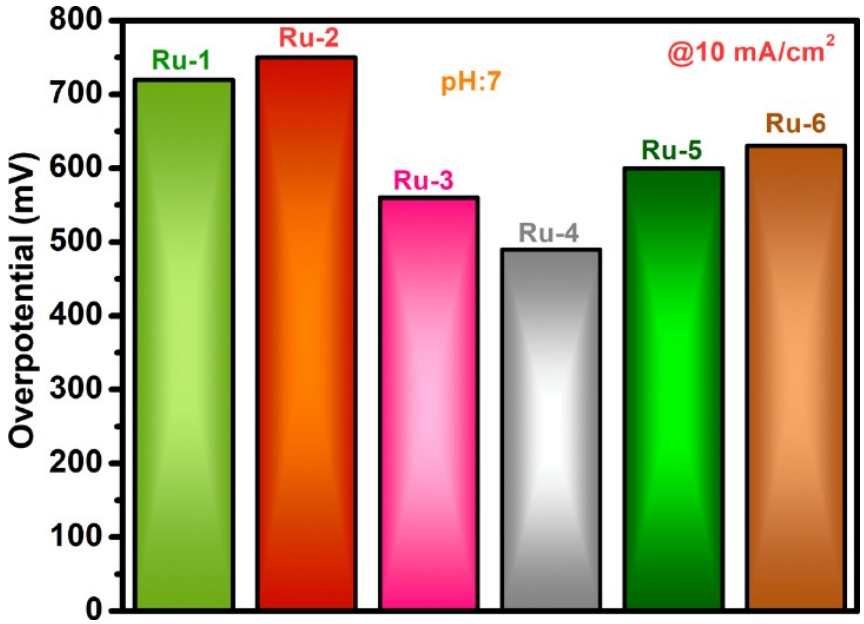

Figure S21: Bar diagram for the overpotential values at 10 mA/cm^2 for all prepared catalyst.

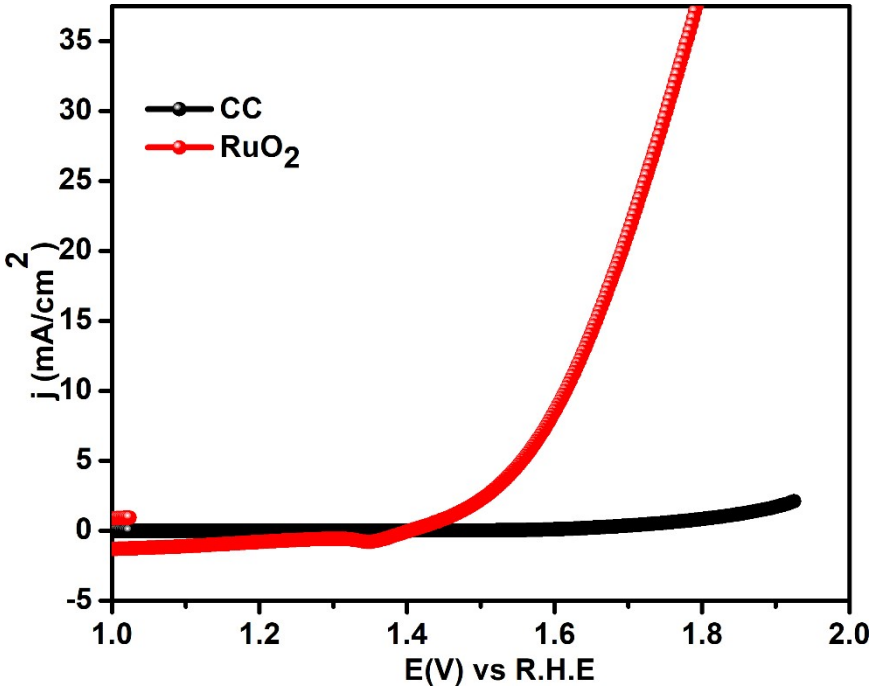

Figure S22: OER study of the state-of-art catalyst and carbon cloth.

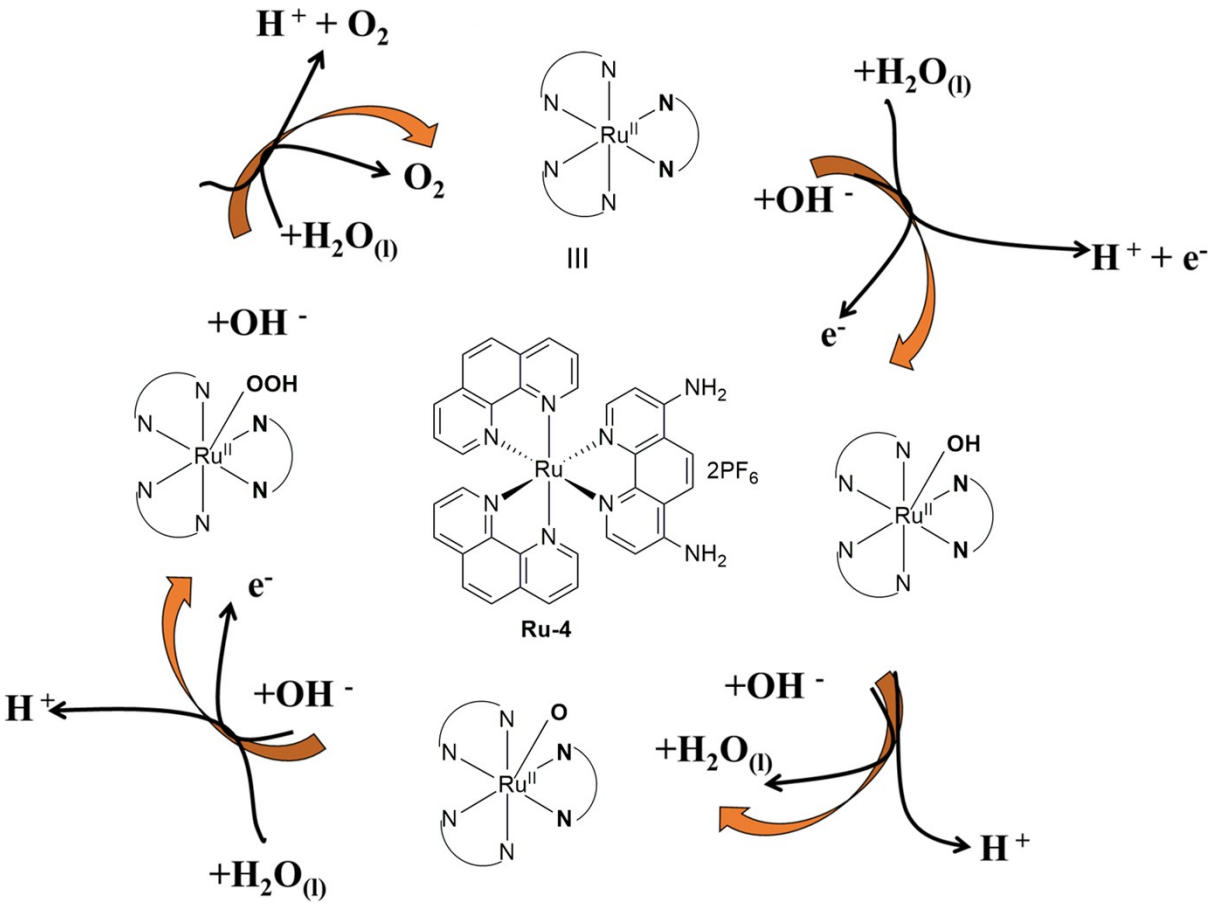

Figure S23: Plausible mechanism of OER for **Ru-4**.

Figure S24: Image of GC-MS setup.

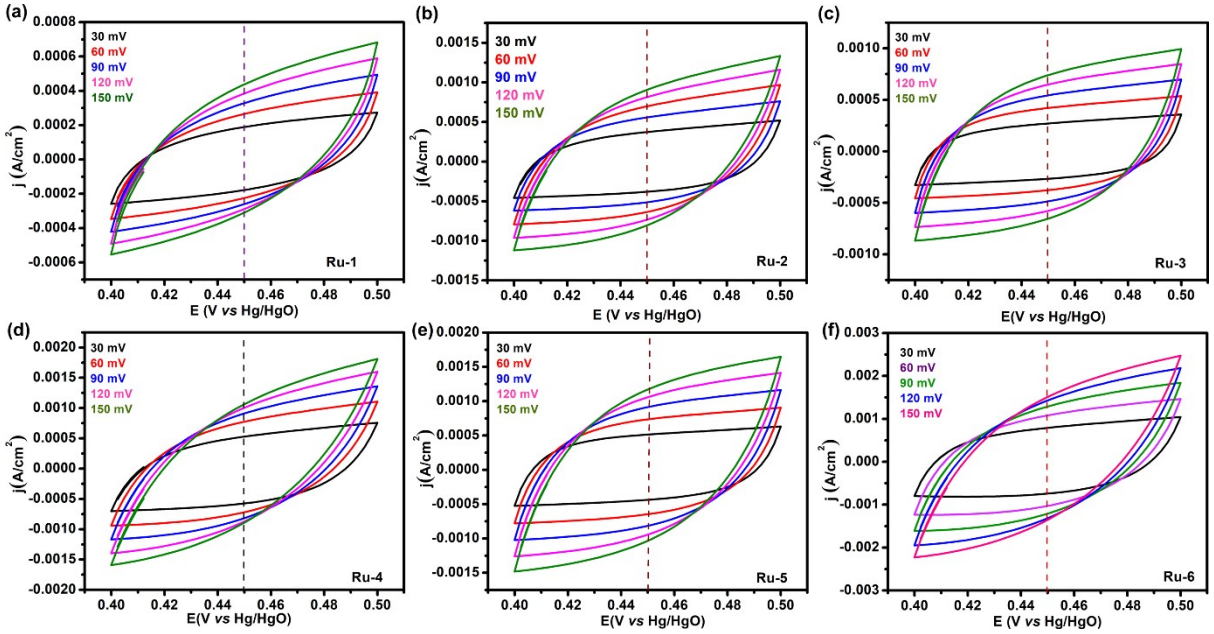

Figure S25: (a-f) scan rate dependent CV curves obtained for calculating the C_{dl} value in non-faradaic region of 0.4-0.5 V *vs* Hg/HgO for **Ru-1** to **Ru-6**.

Table S3: Comparison of OER Overpotential, Tafel slope, R_{ct}, C_{dl}, ECSA and TOF of **Ru-1**, **Ru-2**, **Ru-3**, **Ru-4**, **Ru-5** and **Ru-6**

Catalyst	Overpotential ή@10mA/cm² (mV)	Tafel slope (mV/dec)	R_{ct} ohm	C_{dl} µF/cm²	ECSA	TOF
Ru-1	720	208	16.715	05.72	0.173	$1.27X10^{-5}$
Ru-2	750	253	34.279	06.93	0.143	$2.81X10^{-6}$
Ru-3	560	168	8.650	13.97	0.313	$2.27X10^{-5}$
Ru-4	**490**	**157**	**8.15**	**12.52**	**0.349**	**$4.16X10^{-5}$**
Ru-5	600	176	9.98	11.17	0.279	$1.80X10^{-5}$
Ru-6	630	188	12.90	08.92	0.223	$1.59X10^{-5}$

Table S4: Comparison table with previous reports.

Materials	**Electrolytes**	**Overpotential (mV) at 10 mA cm^{-2}**	**Tafel slope (mV dec^{-1})**	**Stability (V or mA cm^{-2} @h)**	**Reference**
Ru nanoparticles	0.5 M H_2SO_4	202	~70	10 mA cm^{-2} @ 10 h	5
Ru@IrO_x	0.05 M H_2SO_4	282	~69	1.55 V @ 24 h	6
$Ru_2(OH)(OH_2)$		530			7
MWCNT-bpyRutpy	1 M KOH	436	77.2	-	8
cis-[Ru(bpy)(5,5′-dcbpy)$(H_2O)_2$]$^{2+}$	0.1 M HNO_3	-	-	-	9
Ru-1	**0.5 M PBS**	**720**	**208**	-	**This Work**
Ru-2	**0.5 M PBS**	**750**	**253**	-	**This Work**
Ru-3	**0.5 M PBS**	**560**	**168**	-	**This Work**
Ru-4	**0.5 M PBS**	**490**	**157**	**24**	**This Work**
Ru-5	**0.5 M PBS**	**600**	**176**	**-**	**This Work**
Ru-6	**0.5 M PBS**	**630**	**188**	**-**	**This Work**

Computational Studies

The geometry optimization of **Ru-4** was performed with the Gaussian 16 program package using density functional theory (DFT). The B3LYP/6-31G+(d,p)[10] basis set was used for C, H, N, O together with the LANL2DZ[11] for ruthenium. Time-dependent density functional theory (TD-DFT) calculations at the ground-state geometry in acetonitrile were performed in conjunction with the conductor-like polarizable continuum model (CPCM)[12] for acetonitrile with a spin-restricted formalism to examine low-energy excitations at the same level of calculation, which employed for geometry optimizations with 50 number states. Triplet-state TDDFT calculations for complex **Ru-4** were performed using the ground-state optimized geometry, and the UB3LYP/6-31G (d,p) basis set was used for C, H, N, and O

together with the LANL2DZ for Ru. The conductor-like polarizable continuum model (CPCM) for acetonitrile with a spin-unrestricted formalism was employed for singlet–triplet transitions to understand the nature of the weakly emissive states of **Ru-4**

Reference:

1. B. Sen, M. Rabha, S. K. Sheet, D. Koner, N. Saha and Khatua, *Inorg. Chem. Front.* 2021, **8**, 669–683.
2. S. K. Sheet, B. Sen, S. K. Patra, M. Rabha, K. Aguan and S. Khatua, *ACS Appl. Mater. Interfaces* 2018, **10**, 14356–14366.
3. B. Sen, S. K. Patra and S. Khatua, *Inorg. Chem.* 2021, **60**, 19175−19188.
4. E. T. Luis, G. E. Ball, A. Gilbert, H. Iranmanesh, C. W. Newdick and J. E. Beves, *J. Coord. Chem*. 2016, **69**, 1686–1694.
5. J.-Q. Wang, C. Xi, M. Wang, L. Shang, J. Mao, C.-K. Dong, H. Liu, S. A. Kulinich and X.-W. Du, *ACS Catal.*, 2020, **10**, 12575–12581
6. J. Shan, C. Guo, Y. Zhu, S. Chen, L. Song, M. Jaroniec, Y. Zheng and S.-Z. Qiao, *Chem*, 2019, **5**, 445–459
7. Y. Tanahashi, S. Nagai, Y. Tsubonouchi, M. Hirahara, T. Sato, E. A. Mohamed, Z. N. Zahran, K. Saito, T. Yui and M. Yagi, *ACS Appl. Energy Mater*. 2020, **3**, 12172–12184.
8. Z. Wu, Q. Zhang, L. Huang, Y. Xu and D. Tang, *J. Power Sources*, 2021, **488**, 229448.
9. R. Ezhov, A. K. Ravari, A. Page, and Y. Pushkar, *ACS Catal*. 2020, **10**, 5299−5308.
10. A. D. Becke, *J. Chem. Phys.* 1993, **98**, 5648–5652.
11. P. J. Hay and W. R Wadt. *J. Chem. Phys*. 1985, **82,** 299– 310.
12. M. Cossi and V. T. Barone, *J. Chem. Phys*. 2001, **115,** 4708– 4717.